Measuring the Topological Susceptibility in a Fixed Sector: Results for Sigma Models

Irais Bautista[a,b], Wolfgang Bietenholz[a], Arthur Dromard[c], Urs Gerber[a], Christoph P. Hofmann[d], Héctor Mejía-Díaz[a] and Marc Wagner[c]

[a] Instituto de Ciencias Nucleares
Universidad Nacional Autónoma de México
A.P. 70-543, C.P. 04510 Distrito Federal, Mexico

[b] Facultad de Ciencias Físico Matemáticas, Benemérita Universidad Autónoma de Puebla, A.P. 1364, Puebla, Mexico

[c] Goethe-Universität Frankfurt am Main
Institut für Theoretische Physik
Max-von-Laue-Straße 1, D-60438 Frankfurt am Main, Germany

[d] Facultad de Ciencias, Universidad de Colima
Bernal Díaz del Castillo 340, C.P. 28045 Colima, Mexico

For field theories with a topological charge Q, it is often of interest to measure the topological susceptibility $\chi_{\rm t} = (\langle Q^2\rangle - \langle Q\rangle^2)/V$. If we manage to perform a Monte Carlo simulation where Q changes frequently, $\chi_{\rm t}$ can be evaluated directly. However, for local update algorithms and fine lattices, the auto-correlation time with respect to Q tends to be extremely long, which invalidates the direct approach. Nevertheless, the measurement of $\chi_{\rm t}$ is still feasible, even when the entire Markov chain is topologically frozen. We test a method for this purpose, based on the correlation of the topological charge density, as suggested by Aoki, Fukaya, Hashimoto and Onogi. Our studies in non-linear σ-models yield accurate results for $\chi_{\rm t}$, which confirm that the method is applicable. Unfortunately, for increasing volume the wanted signal gets rapidly suppressed, and this method requires huge statistics.

1 Motivation

We are going to address the functional integral formulation of quantum physics in Euclidean space with periodic boundary conditions. For a number of models of interest, the configurations occur in distinct topological sectors, each one characterised by a topological charge $Q \in \mathbb{Z}$. Examples are 2d Abelian gauge theory and 4d Yang-Mills theories. In these cases also fermions may be present, so this class includes the Schwinger model and QCD. Further examples are the $O(N)$ models (non-linear σ-models) in $N-1$ dimensions, and all 2d $CP(N-1)$ models. In the continuum formulation of such models, the charge Q — and therefore the topological sector — cannot be changed by a continuous deformation of the configuration (at finite action). Thus the functional integral splits into distinct integrals for each of the sectors, which are separated by infinite action barriers.

Here we deal with the case where parity symmetry holds, which implies the expectation value $\langle Q \rangle = 0$. Then the topological susceptibility is given by

$$\chi_{\mathrm{t}} = \int d^d x \, \langle q(0) q(x) \rangle = \frac{\langle Q^2 \rangle}{V_{\mathrm{cont}}} \; , \tag{1.1}$$

where q is the topological charge density ($Q = \int d^d x \, q(x)$), and V_{cont} is the volume. This quantity is often of interest; for instance χ_{t} of quenched QCD is relevant for the Witten-Veneziano relation [1], which explains the amazingly heavy mass of the η'-meson as a topological effect.

Clearly, χ_{t} can only be determined on the non-perturbative level. Hence lattice simulations are the appropriate method for this purpose. Strictly speaking, the lattice regularization removes the topological sectors, but there are still sectors separated by barriers of high Euclidean action. So it is possible — and useful — to introduce topological charges in lattice field theory as well, although this involves a slight ambiguity. For comparative studies of different approaches, see Ref. [2].

Here we consider the 1d $O(2)$ model (quantum rotor), as well as the 2d $O(3)$ model (Heisenberg model). In both models we employ the geometric definition [3] of the lattice topological charge density q_x, which has the virtue of automatically providing integer topological charges, as in the continuum, $Q = \sum_x q_x \in \mathbb{Z}$ (x are the lattice sites, which we write as indices, and we always assume periodic boundary conditions).

In our simulations we use the powerful Wolff cluster algorithm [4], which performs non-local update steps of entire spin clusters. Hence our Markov

chains do change Q frequently, so in this specific case $\chi_{\rm t}$ can also be measured directly, without numerical problems.[1]

However, here we are interested in testing the Aoki-Fukaya-Hashimoto-Onogi (AFHO) method [5], which evaluates $\chi_{\rm t}$ based on the density correlations $\langle q_0\, q_x\rangle_{|Q|}$ at large separation x, measured at fixed $|Q|$. This method is still applicable when the only known efficient algorithms proceed in local update steps, which is the situation in most theories involving fermion or gauge fields.[2] It enables the measurement of $\chi_{\rm t}$ even from a Markov chain that is entirely confined to a single topological sector. That may well happen in lattice QCD with light dynamical quarks and a lattice spacing of below 0.05 fm [8]. In light of these prospects for the near future, it is of interest to test the AFHO method systematically.[3]

2 Topological charge density correlation

We are going to investigate the AFHO method, which was derived in Ref. [5], inspired by related considerations by Brower, Chandrasekharan, Negele and Wiese [11]. It deals with the long-distance correlation of the topological charge density q_x at fixed $|Q|$. The topological susceptibility $\chi_{\rm t}$ can be evaluated from the (approximate) relation

$$\begin{aligned} \lim_{x\to\infty}\, \langle q_0\, q_x\rangle_{|Q|} &\approx -\frac{1}{V^2}\left(\langle Q^2\rangle - Q^2 + \frac{V c_4}{2\langle Q^2\rangle}\right) \\ &= -\frac{\chi_{\rm t}}{V} + \frac{1}{V^2}\left(Q^2 - \frac{c_4}{2\chi_{\rm t}}\right)\ , \end{aligned} \tag{2.1}$$

where V is the volume in lattice units. The term

$$c_4 = \frac{1}{V}\Big(3\langle Q^2\rangle^2 - \langle Q^4\rangle\Big) \tag{2.2}$$

is the kurtosis, which measures the deviation from a Gaussian distribution of the topological charges. It tends to be tiny, see *e.g.* Refs. [12] for QCD

[1] In addition, in the 1d $O(2)$ model, the large volume limit of $\chi_{\rm t}$ is known analytically for all the three lattice actions that we are going to consider, cf. Section 3.

[2] Exceptions are 2d pure $U(1)$ gauge theory [6] (which is equivalent to the 1d $O(2)$ model), and specific, purely fermionic models [7].

[3] An alternative concept with the same motivation is sketched in Ref. [9]. For a recent study with a related approach, see Ref. [10]. The procedure of Ref. [11] is more general, but it contains yet another option to determine $\chi_{\rm t}$ from topologically restricted measurements.

results, and in the 1d $O(2)$ model it vanishes exactly in the continuum and infinite volume [13]. In the current context its contribution can be ignored, see Sections 3 and 4.

Eq. (2.1) consists of the leading terms of an expansion in $1/\langle Q^2 \rangle$, therefore $\langle Q^2 \rangle = V \chi_{\rm t}$ should be large. Since $\chi_{\rm t}$ is expected to stabilise in the large volume limit, eq. (2.1) holds up to sub-leading finite size effects. Moreover, its derivation assumes the ratio $|Q|/\langle Q^2 \rangle$ to be small, hence it is favourable to apply this method in sectors of small $|Q|$.

With these assumptions, eq. (2.1) shows that the correlation of the topological charge density in a fixed sector is not expected to vanish over long distances. Instead it is expected to attain a plateau, which depends on $|Q|$: it is slightly negative for $Q = 0$ (obviously, a fluctuation of q_0 has to be compensated elsewhere), but it rises for increasing Q^2.

The AFHO method has been tested previously in the 2-flavour Schwinger model with light chiral fermions [14]. The numerically measured correlations $\langle q_0 \, q_x \rangle_0$ suggest that a conclusive evaluation of $\chi_{\rm t}$ requires large statistics: on a 16×16 lattice it requires $O(10^5)$ configurations. Variants of this method were already applied in 2-flavour QCD, though with a different density [15], and recently also in QCD with $2 + 1$ flavours, with a reduction to sub-volumes [16]. For a precise test, the non-linear σ-models are perfectly suited, since the method can be probed with high statistics, and the results for $\chi_{\rm t}$ can be compared with reliable direct measurements. Synopses of this study were anticipated in two proceeding contributions [17].

3 Results for the 1d $O(2)$ model

We start with the 1d $O(2)$ model, or 1d XY model, which describes a quantum mechanical particle moving freely on the circle S^1, with periodic boundary conditions in Euclidean time x. In continuous time, a trajectory can be described by an angle $\varphi(x)$, with $\varphi(0) = \varphi(L_{\rm cont})$. On the lattice we deal with angles φ_x, $x = 1 \ldots L$ and $\varphi_{L+1} = \varphi_1$.[4] We introduce the nearest site difference

$$\Delta\varphi_x = (\varphi_{x+1} - \varphi_x) \bmod 2\pi \in (-\pi, \pi] \; , \tag{3.1}$$

i.e. the modulo function is defined such that $|\Delta\varphi_x|$ is minimised.

[4] All lattice quantities will be given in lattice units.

This is one of the simplest models with a topological charge, which is given by

$$Q = \frac{1}{2\pi}\int_0^{L_{\rm cont}} dx\,\varphi'(x) \;\; \text{(continuum)}\;, \quad Q = \frac{1}{2\pi}\sum_{x=1}^{L}\Delta\varphi_x \;\; \text{(lattice)}\;, \quad (3.2)$$

where $q(x) = \varphi'(x)/(2\pi)$ is the topological charge density in the continuum, and $q_x = \Delta\varphi_x/(2\pi)$ is its geometrically defined counterpart on the lattice.

The continuum action reads $S_{\rm cont}[\varphi] = \frac{\beta_{\rm cont}}{2}\int_0^{L_{\rm cont}} dx\,\varphi'(x)^2$. In Appendix A we show that relation (2.1) without the kurtosis term,

$$\langle q(0)q(x)\rangle = -\frac{\chi_{\rm t}}{V} + \frac{Q^2}{V^2}\;, \quad (3.3)$$

is exact in this case, and independent of the separation x.

In our numerical study, we are going to consider three lattice actions: the standard action, the Manton action [18] and the constraint action [19],

$$\begin{aligned} S_{\rm standard}[\varphi] &= \beta\sum_{x=1}^{L}(1-\cos\Delta\varphi_x)\;, \quad S_{\rm Manton}[\varphi] = \frac{\beta}{2}\sum_{x=1}^{L}\Delta\varphi_x^2\;, \\ S_{\rm constraint}[\varphi] &= \begin{cases} 0 & \Delta\varphi_x < \delta \quad \forall x \\ +\infty & \text{otherwise} \end{cases}\;. \end{aligned} \quad (3.4)$$

The parameter β (or $\beta_{\rm cont}$) corresponds here to the moment of inertia, and in the last case δ is the constraint angle.

action	ξ	$\chi_{\rm t}$
continuum	$2\beta_{\rm cont}$	$\frac{1}{4\pi^2\beta_{\rm cont}}$
standard	$\left[\ln\frac{\int_{-\pi}^{\pi}d\varphi\;\exp(-\beta(1-\cos\varphi))}{\int_{-\pi}^{\pi}d\varphi\;\exp(-\beta(1-\cos\varphi))\cos\varphi}\right]^{-1}$	$\frac{1}{4\pi^2}\frac{\int_{-\pi}^{\pi}d\varphi\;\varphi^2\exp(-\beta(1-\cos\varphi))}{\int_{-\pi}^{\pi}d\varphi\;\exp(-\beta(1-\cos\varphi))}$
Manton	$\left[\ln\frac{\int_{-\pi}^{\pi}d\varphi\;\exp(-\beta\varphi^2/2)}{\int_{-\pi}^{\pi}d\varphi\;\exp(-\beta\varphi^2/2)\cos\varphi}\right]^{-1}$	$\frac{1}{4\pi^2}\frac{\int_{-\pi}^{\pi}d\varphi\;\varphi^2\exp(-\beta\varphi^2/2)}{\int_{-\pi}^{\pi}d\varphi\;\exp(-\beta\varphi^2/2))}$
constraint	$[\ln(\delta/\sin(\delta))]^{-1}$	$\frac{\delta^2}{12\pi^2}$

Table 1: Closed expressions for the correlation length ξ and the topological susceptibility $\chi_{\rm t}$ in the 1d $O(2)$ model at infinite size, in the continuum and for three lattice actions.

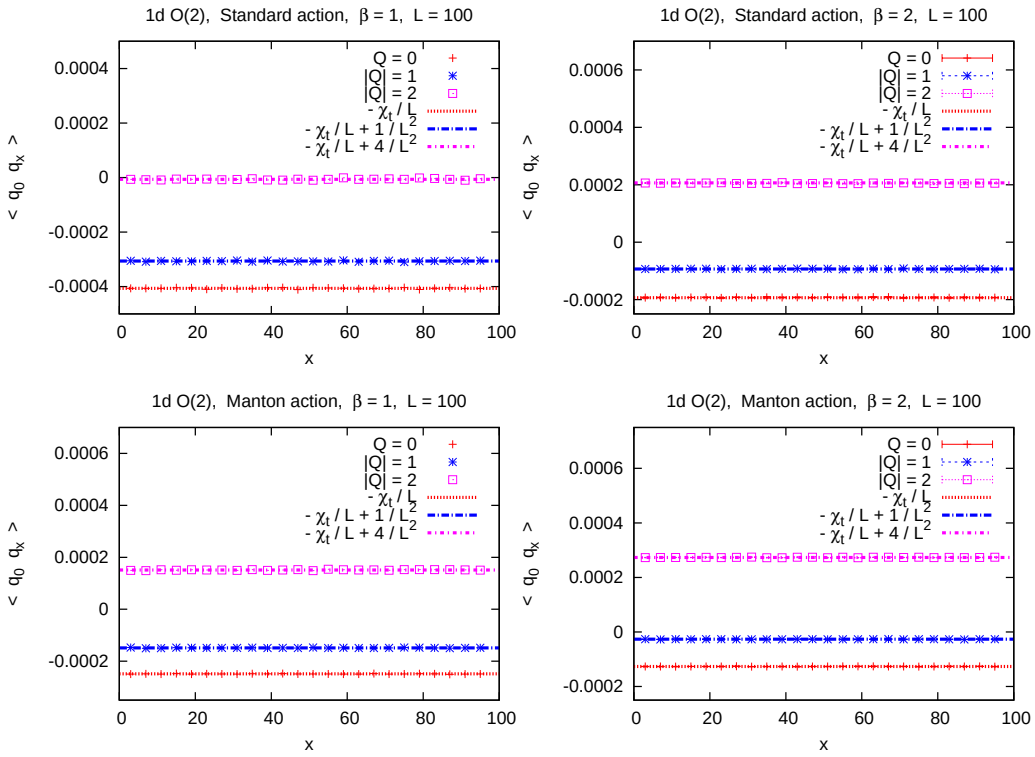

Figure 1: The topological charge density correlation in the 1d $O(2)$ model over a distance of x lattice spacings, at $L = 100$. The plots above refer to the standard action at $\beta = 1$ (on the left), $\beta = 2$ (on the right), which correspond to $\xi = 1.240$, $\langle Q^2 \rangle = 4.063$, and $\xi = 2.779$, $\langle Q^2 \rangle = 1.936$, respectively. The plots below show the same for the Manton action, at $\beta = 1$, $\xi = 2.017$, $\langle Q^2 \rangle = 2.48742$ (on the left), and $\beta = 2$, $\xi = 4.000$, $\langle Q^2 \rangle = 1.266$ (on the right). For comparison, we include in all cases lines for the prediction based on eq. (3.3), where we insert the directly measured values of $\chi_{\rm t}$.

In the thermodynamic limit, $L \to \infty$, the correlation length $\xi = 1/(E_1 - E_0)$ (*i.e.* the inverse energy gap) and $\chi_{\rm t}$ are known analytically, as we summarise in Table 1. The terms for the continuum, the standard and Manton action can be found in Ref. [13], while the terms for the constraint action are derived in Ref. [19].[5] The product $\xi\, \chi_{\rm t}$ is a scaling quantity, *i.e.* a di-

[5]For the continuum action, Ref. [20] discusses the spin correlation function, and its restriction to a single topological sector.

mensionless term composed of observables. In the continuum it amounts to

$$\xi\, \chi_{\rm t}|_{\rm continuum} = \frac{1}{2\pi^2}\ . \tag{3.5}$$

This value is attained for the lattice actions in the limit $\beta \to \infty$ and $\delta \to 0$, respectively, which reveals a facet of universality even in one dimension. The corresponding scaling behaviour is discussed in Refs. [13,19,21]. In particular, the Manton action scales excellently, since it is classically perfect.

Figure 1 shows examples for numerically measured correlations $\langle q_0\, q_x\rangle_{|Q|}$, using the standard action and the Manton action, at $L = 100$, and $\beta = 1$ and 2. We see that the numerical data agree very well with the predicted plateau values; no deviation is visible. The same holds for the constraint action at $\delta = 2\pi/3$, $L = 50$, and at $\delta = 1$, $L = 100$, as Figure 2 shows.

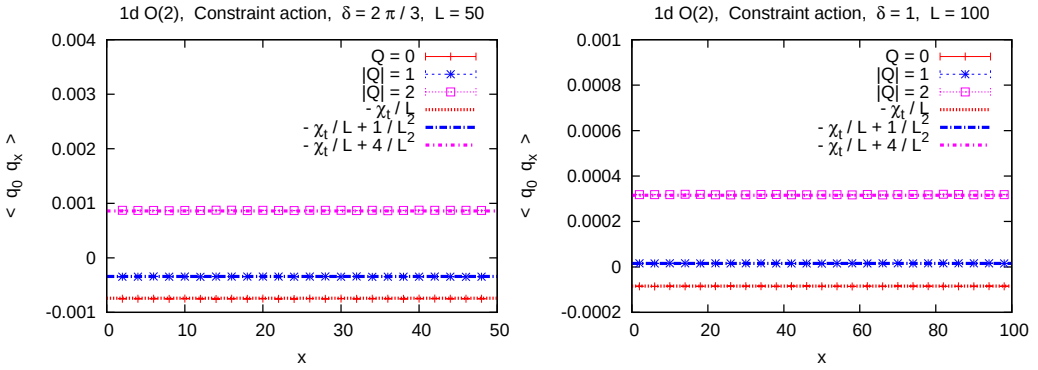

Figure 2: The same as in Figure 1, but now for the constraint action at $\delta = 2\pi/3$, $L = 50$, $\xi = 1.132$, $\langle Q^2\rangle = 1.852$ (on the left), and $\delta = 1$, $L = 100$, $\xi = 5.793$, $\langle Q^2\rangle = 0.844$ (on the right). Again we compare the data to the prediction based on eq. (3.3), where we insert the directly measured $\chi_{\rm t}$.

Hence we confirm that the method works, but for a precise analysis we evaluate $\chi_{\rm t}$ from each of these measured correlation plateaux; they are fitted to a constant in the range $2 \ldots L-2$. The condition of a correlation over a "large distance" turns out to be extremely mild in this case (that was different in the corresponding study of the 2-flavour Schwinger model [14]). The reason for this virtue in the 1d $O(2)$ model is discussed in Appendix A.

In order to probe the AFHO method close to the continuum limit, we proceed to $\beta = 4$, where the correlation length is increased to $\xi = 6.8$ for the standard lattice action, and to $\xi = 8.0$ for the Manton action. In the

range $L = 150 \ldots 400$, and for $|Q| = 0,\ 1,\ 2$, this leads to the results for $\chi_{\rm t}$ illustrated in Figure 3. For the Manton action we obtain precise agreement with the theoretical $\chi_{\rm t}$ value in all cases. For the standard action we observe small deviations up to a few permille, which are suppressed for $|Q| \leq 1$, and for $|Q| = 2$ they are reduced as L increases.

These tiny lattice artifacts are revealed due to extremely large statistics: for each parameter set, at least $5 \cdot 10^9$ measurements have been performed. This yields very precise results, and illustrates the convergence towards the theoretical $\chi_{\rm t}$ value for increasing $\langle Q^2 \rangle$ (or equivalently L).

However, such a huge statistics is usually not available in higher dimensional models. As a more realistic benchmark, we now consider the constraint action with $\delta = 2\pi/3,\ 1.5,\ 1$, in the range $L = 50 \ldots 400$, with 10^7 measurements in each case. The results are illustrated in Figure 4. They confirm that this enables the determination of $\chi_{\rm t}$ to two digits with the AFHO method, as one expects based on Figure 3. In addition, we see that the values obtained at $|Q| = 2$ converge to the correct result if L increases, such that $\langle Q^2 \rangle$ is getting sufficiently large.

The detailed high precision results for the standard and Manton action are given in Tables 2 and 3. Table 4 adds examples for the measured values of the kurtosis, which was defined in eq. (2.2). For the standard action it differs from 0 well beyond the statistical uncertainty. This is a lattice artifact, since c_4 approaches 0 for increasing β (but this trend is not manifest for increasing L), in agreement with Appendix A. Hence Table 4 also confirms the excellent scaling behaviour of the Manton action.

β	L	$Q = 0$	$\lvert Q\rvert = 1$	$\lvert Q\rvert = 2$	$\lvert Q\rvert = 3$	$\lvert Q\rvert = 4$	direct
1	100	0.04067(2)	0.04066(2)	0.04060(3)	0.04050(3)	0.04064(5)	0.040635(3)
2	100	0.019277(7)	0.019325(7)	0.01946(1)	0.01966(2)	0.01987(6)	0.019364(1)
4	150	0.007537(2)	0.007552(3)	0.007589(5)	0.00773(2)	0.00746(8)	0.0075543(3)
	200	0.007541(3)	0.007549(3)	0.007578(5)	0.00761(1)	0.00768(4)	0.0075543(3)
	250	0.007544(3)	0.007548(4)	0.007562(5)	0.00756(1)	0.00759(3)	0.0075543(3)
	300	0.007546(4)	0.007548(4)	0.007556(6)	0.00759(1)	0.00756(2)	0.0075542(3)
	350	0.007546(4)	0.007550(4)	0.007573(6)	0.00755(1)	0.00761(2)	0.0075543(3)
	400	0.007548(4)	0.007553(5)	0.007561(7)	0.007555(9)	0.00756(2)	0.0075547(3)

Table 2: The values of $\chi_{\rm t}$ determined by the AFHO method in the lattice 1d $O(2)$ model with the standard action, in the sectors $|Q| = 0 \ldots 4$. For comparison we also display the results of direct $\chi_{\rm t}$ measurements.

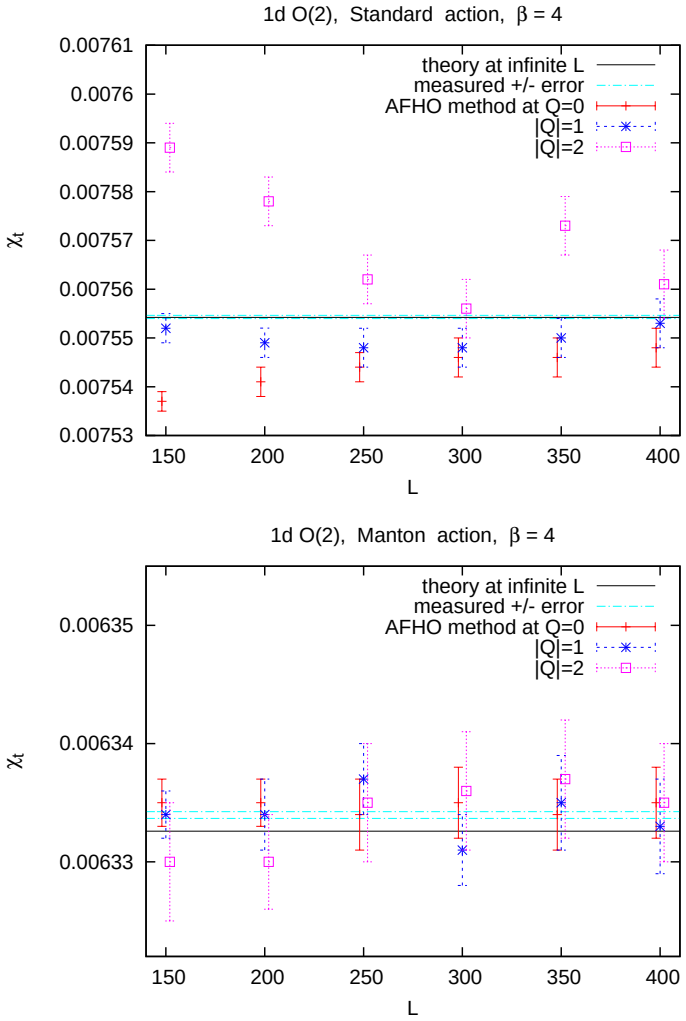

Figure 3: The topological susceptibility χ_t in the 1d $O(2)$ model for the standard action (above) and for the Manton action (below), both at $\beta = 4$. We show the theoretical value at $L = \infty$, the directly measured value (at $L = 400$), and the values obtained from the AFHO method in the range $L = 150 \ldots 400$, in the sectors $|Q| = 0,\ 1,\ 2$. For the standard action, there are permille level deviations from the predicted value, in particular for $|Q| = 2$, but they are suppressed for increasing L. For the Manton action all results coincide to an impressive precision, even down to $L = 150$.

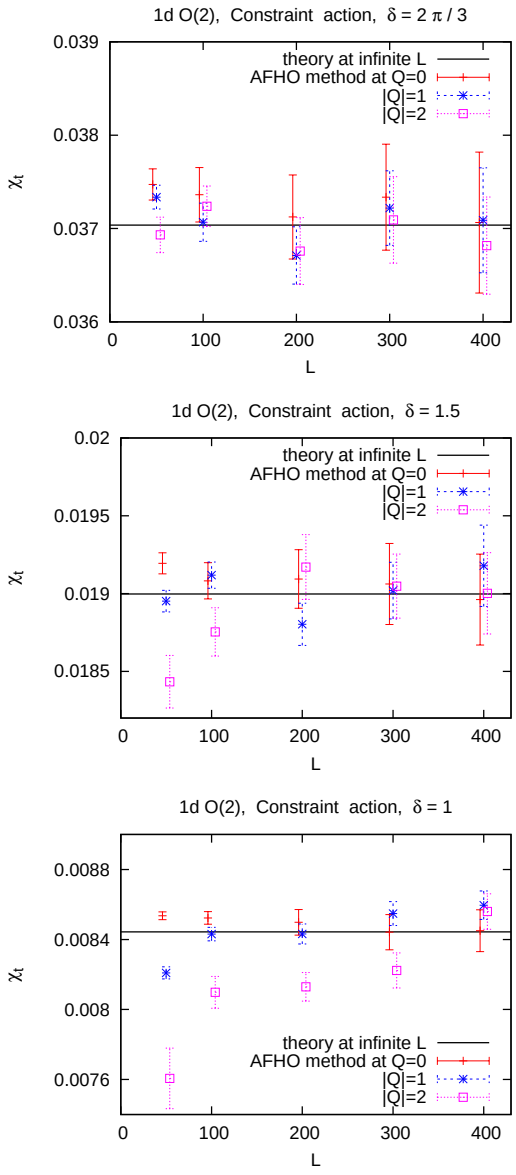

Figure 4: The topological susceptibility $\chi_{\rm t}$ in the 1d $O(2)$ model for the constraint action at $\delta = 2\pi/3$, $\delta = 1.5$ and $\delta = 1$. We show values obtained from the AFHO method in the range $L = 50 \ldots 400$, in the sectors $|Q| = 0,\ 1,\ 2$. In the smallest volumes there are significant deviations, in particular for $|Q| = 2$, which are suppressed as L increases.

β	L	$Q=0$	$\|Q\|=1$	$\|Q\|=2$	$\|Q\|=3$	$\|Q\|=4$	direct
1	100	0.024889(7)	0.024879(9)	0.02487(1)	0.02483(2)	0.02500(3)	0.024874(1)
2	100	0.012665(3)	0.012666(4)	0.012664(7)	0.01275(2)	0.01256(9)	0.0126643(6)
4	150	0.006335(2)	0.006334(2)	0.006330(5)	0.00634(2)	0.0066(1)	0.0063347(3)
	200	0.006335(2)	0.006334(3)	0.006330(4)	0.00634(1)	0.00665(5)	0.0063346(3)
	250	0.006334(3)	0.006337(3)	0.006335(5)	0.00636(1)	0.00636(3)	0.0063342(3)
	300	0.006334(3)	0.006331(3)	0.006336(5)	0.006336(9)	0.00640(2)	0.0063342(3)
	350	0.006334(3)	0.006335(4)	0.006337(5)	0.006333(9)	0.00638(2)	0.0063344(3)
	400	0.006335(3)	0.006333(4)	0.006335(5)	0.006346(9)	0.00635(2)	0.0063340(3)

Table 3: Results analogous to Table 2, but now for the Manton action.

L	β	standard action	Manton action	constraint action $\delta=2\pi/3$	constraint action $\delta=1$
100	2	−0.00033(2)	−0.00000004(470)	0.0015(9)	0.00006(4)
200	4	−0.000039(4)	−0.0000002(25)	0.0009(11)	0.00010(5)
300		−0.000040(5)	−0.0000009(37)	0.0021(17)	0.00005(8)
400		−0.000040(7)	−0.000002(50)	0.0015(26)	0.00008(13)

Table 4: Some numerical values of the kurtosis $c_4 = (3\langle Q^2\rangle^2 - \langle Q^4\rangle)/L$ in the 1d $O(2)$ model. These results show that the significant deviations from 0, which are observed in the standard action, are due to lattice artifacts (not finite size effects).

4 Results for the 2d $O(3)$ model

We proceed to field theory, and more specifically to the 2d $O(3)$ model (or Heisenberg model), with periodic boundary conditions in both directions. In its lattice formulation a classical spin variable of unit length is attached to each lattice site x, $\vec{e}_x \in S^2$.

Regarding the topological charge, we consider sets of three neighbouring spins. In our case the lattice consists of quadratic plaquettes, and each plaquette is divided into two triangles (the cutting diagonal has an alternating orientation between nearest neighbour plaquettes). Each of these triangles carries such a set of three spins. They are connected on the sphere S^2 by

the arcs of minimal length to form a spherical triangle. In each plaquette, the normalised sum of these two oriented spherical triangles (the total solid angle), $q_x = A(\vec{e}_x, \vec{e}_{x+\hat{1}}, \vec{e}_{x+\hat{2}}, \vec{e}_{x+\hat{1}+\hat{2}})/(4\pi)$, is the topological charge density.

If we sum over all plaquettes, and thus over all triangles, we obtain the geometrically defined topological charge

$$Q = \sum_x q_x = \frac{1}{4\pi} \sum_x A(\vec{e}_x, \vec{e}_{x+\hat{1}}, \vec{e}_{x+\hat{2}}, \vec{e}_{x+\hat{1}+\hat{2}}) \in \mathbb{Z} \ . \tag{4.1}$$

This definition, which was advocated in Ref. [3], has the virtue of providing integer Q values for all configurations (except for a subset of measure zero), just like eq. (3.2). It counts how many times (and with which orientation) these triangles cover the sphere. Fully explicit formulae are given *e.g.* in Ref. [19].

The standard lattice action reads

$$S_{\text{standard}}[\vec{e}] = \beta \sum_{x,\mu} (1 - \vec{e}_x \cdot \vec{e}_{x+\hat{\mu}}) \ , \tag{4.2}$$

where μ runs from 1 to 2, $\hat{\mu}$ is the unit vector in μ-direction, and $\beta > 0$. Figure 5 shows the topological charge density correlation $\langle q_0 \, q_{|x|} \rangle$ at $\beta = 1$, measured in the sectors $|Q| = 0, \ 1, \ 2$, on $L \times L$ lattices of size $L = 12$ and $L = 16$. The measurements are carried out parallel to the axes, and the spin separation proceeds in steps of two lattice units, due to the alternating triangularisation in the definition of q_x.

The horizontal lines are the expected plateau values according to eq. (3.3). Again we inserted the directly measured values of $\chi_t = \langle Q^2 \rangle / V$; they are very precise, thanks to the use of a cluster algorithm [4], which provided a statistics of $O(10^7)$ well thermalised and decorrelated measurements.[6]

The plots clearly confirm the qualitatively expected picture. We further confirm the observation of Section 3 that the condition of a large separation is quite harmless: for the separation of four lattice spacings, the plateau value is already well attained.[7]

[6] This model is sometimes considered topologically ill, because $\chi_{\text{t}} \, \xi^2$, which is supposed to be the scaling term, diverges logarithmically in the continuum limit. In the integral representation of eq. (1.1), this effect emerges at distance $x = 0$; at finite distances, the topological charge density correlation is actually a controlled quantity [19]. Here we determine χ_{t} with different methods at fixed ξ, so this defect does not affect our study.

[7] In the plateau fits of the 2d $O(3)$ model data for $\langle q_0 \, q_{|x|} \rangle$ that we present in this section, we skip about $2 \ldots 6$ points at the boundaries. This is done in each case such that we capture optimally the asymptotic value at large separation.

For a quantitative analysis, we perform individual fits of the data to a constant in one sector; each fit yields a value of the topological susceptibility $\chi_{\rm t}$. These results are confronted with the directly measured values in Table 5. In addition we consider combined fits in two or three sectors. As theory predicts, the lowest-$|Q|$ sectors are most reliable. In fact, the evaluation of $\chi_{\rm t}$ based on $\langle q_0\, q_{|x|}\rangle_{|Q|}$ is successful to an accuracy of a few percent in these cases. However, Figure 5 also shows that this method is rapidly getting difficult to apply when L increases: then the values of $\langle q_0\, q_{|x|}\rangle_{|Q|}$ become tiny, and thus hard to distinguish from zero, and from each other.

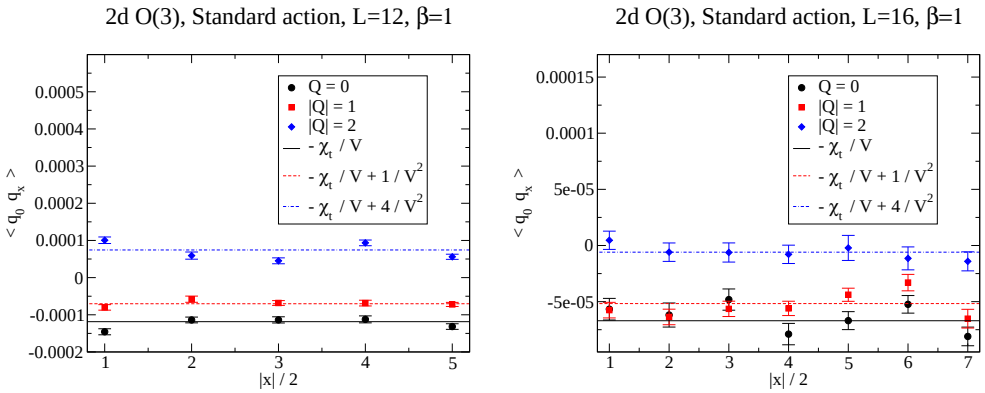

Figure 5: The topological charge density correlation in the 2d $O(3)$ model, with the standard lattice action at $\beta = 1$, which corresponds to $\xi \simeq 1.3$. We show data measured on $L \times L$ lattices, $L = 12$ and 16, in the sectors $|Q| = 0$, 1, 2, compared to lines for the values according to eq. (3.3), with the directly measure susceptibility $\chi_{\rm t}$.

This is a case of strong coupling; $\beta = 1$ leads to a correlation length of $\xi \simeq 1.3$ (at large L). Hence the volumes that we used can be considered large, but the lattice is coarse. In order to probe the AFHO method closer to the continuum limit, we now proceed to a different setting. We move to the constraint action, which is defined in analogy to eq. (3.4), cf. Ref. [19],

$$S_{\rm constraint}[\vec{e}\,] = \begin{cases} 0 & \vec{e}_x \cdot \vec{e}_{x+\hat{\mu}} > \cos\delta \quad \forall x,\, \mu \\ +\infty & \text{otherwise} \end{cases} \quad . \tag{4.3}$$

We set the constraint angle to $\delta = 0.55\,\pi$, which corresponds to a correlation length of $\xi \simeq 3.6$. Accordingly, we now consider larger square lattices, with $L = 16$ and $L = 32$. Figure 6 shows the topological charge correlations in

L	$\|Q\|$	χ_t (fixed $\|Q\|$)	χ_t (direct)
12	0	0.018(1)	0.01707(4)
	1	0.0170(5)	
	0 and 1	0.0174(5)	
	2	0.018(2)	
	0 to 2	0.0175(6)	
16	0	0.016(2)	0.01715(3)
	1	0.017(2)	
	0 and 1	0.0164(10)	
	2	0.0174(4)	
	0 to 2	0.0167(7)	

Table 5: Evaluation of the topological susceptibility in the 2d $O(3)$ model on $L \times L$ lattices, with the standard action at $\beta = 1$. We display results obtained from fits to the topological charge density correlation in sector $|Q|$, or combined fits in several sectors. This is compared to the direct measurement as $\langle Q^2 \rangle / V$, which is very precise. The results by both methods are compatible within the errors.

this case, and Table 6 contains the quantitative results, in analogy to the presentation for the standard action.

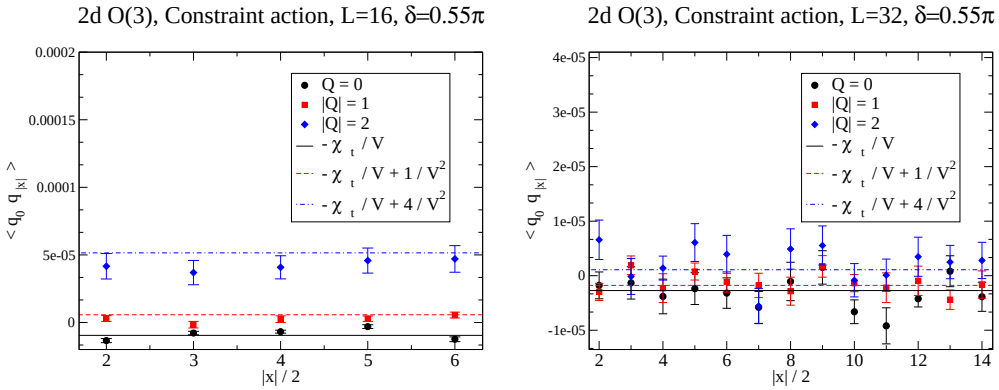

Figure 6: Plots analogous to Figure 5, now for the constraint action at $\delta = 0.55\,\pi$, which corresponds to $\xi \simeq 3.6$, and with lattice sizes $L = 16$ and $L = 32$.

These plots show again that the condition of a larger separation $|x|$ is not a practical problem. However, despite the statistics of $O(10^7)$ measurements,

L	$\|Q\|$	$\chi_{\rm t}$ (fixed $\|Q\|$)	$\chi_{\rm t}$ (direct)
16	0	0.0021(5)	0.0024420(10)
	1	0.0032(3)	
	0 and 1	0.0024(4)	
	2	0.0048(5)	
	0 to 2	0.0024(3)	
32	0	0.0035(8)	0.0027892(15)
	1	0.0022(6)	
	0 and 1	0.0027(5)	
	2	0.0018(10)	
	0 to 2	0.0025(5)	

Table 6: Evaluation of the topological susceptibility in the 2d $O(3)$ model on $L \times L$ lattices, with the constraint action at $\delta = 0.55\,\pi$, where $\xi \simeq 3.6$. We display results from fits to the topological charge density correlation in sector $|Q|$, or combined fits in several sectors. Comparison to the direct measurement shows that the AFHO method is less successful than in the examples of Table 5, since larger volumes are involved; in general, only the first digit is reliable.

the AFHO method does run into considerable trouble in reproducing the directly measured χ_t values beyond one digit. This is mostly a consequence of the larger volumes involved; they suppress the signal, which is relevant to extract χ_t in this indirect manner.

Let us finally take a large step to a numerical experiment very close to the continuum limit: it is performed with the standard lattice action at $\beta = 1.5$, on square lattices with $L = 16 \ldots 128$; at large L, this corresponds to $\xi \simeq 9.5$. Figure 7 shows the results for $\chi_{\rm t}$ up to $L = 84$, based on the topological charge correlations in the sectors $|Q| = 0$, 1, 2, and by direct measurement. As L increases, the latter converges well at $L \geq 32$. The results by the AFHO method move towards the directly measured value, and get close to it at $L = 40$. Here the range $L \approx 40 \ldots 60$ is optimal for its application. As we increase L further, we face again the problem that the tiny signal, which matters for $\chi_{\rm t}$, gets lost in the statistical noise. For $|Q| = 1$, 2 this happens already at $L \geq 64$, only at $Q = 0$ the method still leads to useful results up to $L = 84$. The numerical values are added in Table 7 (for completeness we include a result at $L = 128$, although it has an error of 42 %).

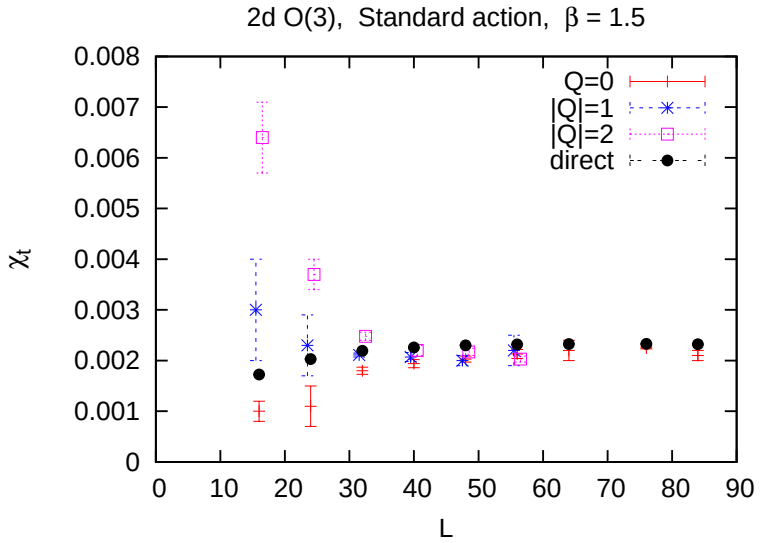

Figure 7: The topological susceptibility χ_t for the standard action at $\beta = 1.5$, on $L \times L$ lattices with $L = 16 \ldots 84$ (with $\xi \simeq 9.5$ at large L). The directly measured values stabilise for $L \geq 32$ (its errors are too small to be visible in this plot), and the AFHO results approximate it well in the regime $L = 40 \ldots 84$. For smaller L, this method suffers from significant finite size effects, and for larger L the signal for the determination of χ_t is too small for a good numerical resolution.

5 Conclusions

We have investigated the AFHO method [5] for the evaluation of the topological susceptibility χ_t based on the correlation of the topological charge density. Amazingly, this method allows — in principle — for a measurement of χ_t even within a fixed topological sector, and $Q = 0$ is most promising.

In our Monte Carlo study of 1d and 2d non-linear σ-models, we could apply a cluster algorithm, which performs non-local update steps. Hence it does not get stuck in a topological sector and it provides precise results for χ_t by direct measurement. In most other models of quantum field theory, especially in almost all models with fermions or gauge fields, such an efficient algorithm is not known. Hence one resorts to local update algorithms, where the Markov chain tends to get stuck in a topological sector, in particular as one approaches the continuum limit. So in all those cases the indirect AFHO

L	$Q=0$	$\|Q\|=1$	$\|Q\|=2$	direct
16	0.0010(2)	0.003(1)	0.0064(7)	0.001725(1)
24	0.0011(4)	0.0023(6)	0.0037(3)	0.002031(3)
32	0.00180(7)	0.00211(4)	0.00248(8)	0.002192(2)
40	0.00194(8)	0.00207(9)	0.0022(1)	0.002258(3)
48	0.00203(6)	0.0020(1)	0.00217(7)	0.002301(1)
56	0.00213(9)	0.0022(3)	0.00203(6)	0.002318(4)
64	0.0022(2)			0.002325(2)
76	0.00225(2)			0.002329(3)
84	0.0021(1)			0.002323(3)
128	0.0019(8)			0.002292(9)

Table 7: Results for $\chi_{\rm t}$ with the standard lattice action at $\beta = 1.5$, on $L \times L$ lattices. The data in specific sectors are based on the AFHO method (we leave the table empty in cases where the signal got lost in the statistical noise).

method could be of interest.

Therefore we have tested its applicability and reliability. The outcome is first of all that the method as such works; in some cases it provided results, which are correct to 2 or 3 digits. Hence situations do exist, where the approximations in the derivation of formula (3.3) (in particular including order $O(1/V^2)$ incompletely, and neglecting all terms of $O(1/V^3)$) can be justified, as we could confirm on the non-perturbative level.

Regarding the limitations of the applicability range, we note that — for the models studied here — the theoretical condition of measuring the correlation "at larger separation" turned out not to be worrisome in practice. However, the AFHO method generally runs into trouble as the volume V increases. Then the crucial signal in $\langle q_0\, q_{|x|}\rangle_{|Q|}$ is suppressed with a factor $1/V$. If we want the correlation length to be clearly larger than the lattice spacing (so that lattice artifacts are under control), we need a sizable lattice to keep the finite size effects under control as well. With these conflicting requirements, even in our 2d test model, and despite a huge statistics, the method did not work well anymore.

The relevant observation is that the AFHO method, which is based on topologically restricted measurements, is plagued by unusually persistent finite size effects. In usual settings, the latter are exponentially suppressed,

i.e. they are $\propto \exp(-\text{const.}\, L/\xi)$, and quite small if $L/\xi \gtrsim 4$. However, topologically restricted numerical measurements are very sensitive to finite size effects: we recall that relation (2.1) is a truncated polynomial expansion in $1/V$, but we can also refer directly to the large ratios L/ξ, which were used all over this study: *e.g.* in the upper plot of Figure 3 it amounts to $L/\xi > 22$, which would usually make finite size effects negligible, but here they are significant. This property calls for a larger size L. In turn, that causes problems in extracting the subtle effect, which is relevant for the indirect determination of $\chi_{\rm t}$.

That issue might be the bottleneck for the prospects to apply the AFHO method in higher dimensions. However, there requirement of a large box size L is expected to be relaxed, since the truncated terms are $1/V$-suppressed. Indeed, the plots in Figure 6 on the left, and in Figure 7, show that in two dimensions good results are obtained even at $L/\xi \approx 4$. Therefore this method could be considered also in 4d theories, which may involve gauge and fermion fields, such as QCD. In that framework a new variant has recently been tested [16]. It might be worthwhile exploring also the applicability of the original form, although a tiny signal has to be resolved (the inclusion of all-to-all correlations could be necessary). A next step would be a test in 4d $SU(2)$ Yang-Mills theory.

Acknowledgements Lilian Prado has worked on this project at an early stage. We also thank Christopher Czaban and Philippe de Forcrand for interesting discussions. This work was supported in part by the Mexican *Consejo Nacional de Ciencia y Tecnología* (CONACYT) through project 155905/10, by DGAPA-UNAM, grant IN107915, and by the *Helmholtz International Center for FAIR* within the framework of the LOEWE program launched by the State of Hesse. A.D. and M.W. acknowledge support by the Emmy Noether Programme of the DFG (German Research Foundation), grant WA 3000/1-1, and C.P.H. acknowledges support through the project *Redes Temáticas de Colaboración Académica 2013,* UCOL-CA-56.

A Topological charge density correlation in the continuum 1d $O(2)$ model

The key quantity of this work is the correlation function of the topological charge density. In this appendix we compute it analytically for the 1d $O(2)$ model, formulated in continuous Euclidean time x, with periodicity length L. For this purpose, it is useful to include a θ-term in the action,

$$S[\varphi] = \frac{\beta_{\rm cont}}{2} \int_0^{L_{\rm cont}} dx\, \varphi'(x)^2 - {\rm i}\theta Q[\varphi] \ . \tag{A.1}$$

In the canonical formulation of quantum mechanics, the corresponding Hamilton operator, its energy eigenfunctions and eigenvalues read [13]

$$\hat{H} = \frac{1}{2\beta_{\rm cont}} \Big(\hat{p} - \frac{\theta}{2\pi}\Big)^2 \ , \ \langle\varphi|n\rangle = \frac{1}{\sqrt{2\pi}}\, e^{{\rm i}n\varphi} \ , \ E_n = \frac{1}{2\beta_{\rm cont}} \Big(n - \frac{\theta}{2\pi}\Big)^2 \ , \tag{A.2}$$

where $\hat{p} = -{\rm i}\frac{\partial}{\partial\varphi}$ and $n \in \mathbb{Z}$. The operator for the topological charge density is given by

$$\hat{q} \ = \ \frac{1}{2\pi}[\hat{H}, \hat{\varphi}] = \frac{1}{2\pi\beta_{\rm cont}} \Big(- \frac{\partial}{\partial\varphi} + {\rm i}\frac{\theta}{2\pi}\Big) \ . \tag{A.3}$$

This operator is *anti-Hermitian* (due to the Euclidean time derivative of the Hermitian operator $\hat{\varphi}$), with the matrix elements

$$\langle m|\hat{q}|n\rangle = \frac{1}{(2\pi)^2\beta_{\rm cont}} \int_{-\pi}^{\pi} d\varphi\, e^{-{\rm i}m\varphi} \Big(- \frac{\partial}{\partial\varphi} + {\rm i}\frac{\theta}{2\pi}\Big)\, e^{{\rm i}n\varphi} = \frac{{\rm i}(\theta - 2\pi n)}{(2\pi)^2\beta_{\rm cont}}\, \delta_{mn} \ .$$

Hence the expectation value

$$\langle q(x)\rangle = \frac{1}{Z(\theta)} \frac{\rm i}{(2\pi)^2\beta_{\rm cont}} \sum_{n\in\mathbb{Z}} (\theta - 2\pi n)\, e^{-E_n L_{\rm cont}} \ , \ \text{with } Z(\theta) = \sum_{n\in\mathbb{Z}} e^{-E_n L_{\rm cont}}$$

is imaginary in general (of course it vanishes at $\theta = 0$).

Therefore the corresponding correlation function is in general *negative,*[8]

$$\begin{aligned} \langle q(0)q(x)\rangle \ &= \ \frac{1}{Z(\theta)} \sum_{m,n\in\mathbb{Z}} \langle m|\hat{q}|n\rangle\, \langle n|\hat{q}|m\rangle\, e^{-E_n x - E_m\,(L_{\rm cont} - x)} \\ &= \ -\frac{1}{Z(\theta)} \frac{1}{(2\pi)^4\beta_{\rm cont}^2} \sum_{n\in\mathbb{Z}} (\theta - 2\pi n)^2\, e^{-E_n L_{\rm cont}} \ . \end{aligned} \tag{A.4}$$

[8] In field theoretic models, the correlation of the topological charge density over large distance is known to be negative as well [22].

It is remarkable that this correlation is independent of x, if $x/L_{\rm cont} \notin \mathbb{Z}$ (this condition allows us to insert a unit factor $\sum_n |n\rangle\langle n|$ between the end-points).

The vacuum angle θ enables also the computation of the topologically restricted partition function,

$$Z_Q = \frac{1}{2\pi}\int_{-\pi}^{\pi} d\theta\, Z(\theta)\, e^{-{\rm i}Q\theta} = \frac{1}{2\sqrt{\pi\alpha}} e^{-Q^2/(4\alpha)} \ , \quad \alpha = \frac{L}{8\pi^2\beta_{\rm cont}} \ ,$$

and correlation function,

$$\begin{aligned} \langle q(0)q(x)\rangle_Q &= \frac{1}{2\pi Z_Q}\int_{-\pi}^{\pi} d\theta\, Z(\theta)\langle q(0)q(x)\rangle\, e^{-{\rm i}Q\theta} \\ &= -\frac{1}{(2\pi)^5\beta_{\rm cont}^2 Z_Q}\int_{-\infty}^{\infty} d\theta\, \theta^2\, e^{-\alpha\theta^2-{\rm i}\theta Q} \\ &= \frac{1}{32\pi^4\beta_{\rm cont}^2\alpha}\Big(-1+\frac{Q^2}{2\alpha}\Big) \ . \end{aligned} \tag{A.5}$$

Finally we insert α and $\chi_{\rm t} = \alpha L_{\rm cont}/2$ (cf. Table 1) to arrive at

$$\langle q(0)q(x)\rangle_Q = -\frac{\chi_{\rm t}}{L_{\rm cont}} + \frac{Q^2}{L_{\rm cont}^2} \ . \tag{A.6}$$

Also the topologically restricted correlation function is constant in x, which explains that the data in Section 3 attain the plateau values immediately.

Moreover, we see that eq. (3.3) is *exact* in this specific case, which is consistent with the fact that the kurtosis vanishes [13]. Therefore, in our numerical study presented in Section 3, the only issue are lattice artifacts, and even they turned out to be mild.

References

[1] E. Witten, *Nucl. Phys.* **B 156** (1979) 269. G. Veneziano, *Nucl. Phys.* **B 159** (1979) 213.

[2] K. Cichy, A. Dromard, E. Garcia-Ramos, K. Ottnad, C. Urbach, M. Wagner, U. Wenger and F. Zimmermann, arXiv:1411.1205 [hep-lat]. Y. Namekawa, arXiv:1501.06295 [hep-lat].

[3] B. Berg and M. Lüscher, *Nucl. Phys.* **B 190** (1981) 412.

[4] U. Wolff, *Phys. Rev. Lett.* **62** (1989) 361.

[5] S. Aoki, H. Fukaya, S. Hashimoto and T. Onogi, *Phys. Rev.* **D 76** (2007) 054508 [arXiv:0707.0396 [hep-lat]].

[6] R. Sinclair, *Phys. Rev.* **D 45** (1992) 2098.

[7] S. Chandrasekharan and U.-J. Wiese, *Phys. Rev. Lett.* **83** (1999) 3116 [cond-mat/9902128].

[8] M. Lüscher, *JHEP* **1008** (2010) 071 [arXiv:1006.4518 [hep-lat]].

[9] Ph. de Forcrand, M. García Pérez, J.E. Hetrick, E. Laermann, J.F. Lagae and I.O. Stamatescu, *Nucl. Phys. (Proc. Suppl.)* **73** (1999) 578 [hep-lat/9810033].

[10] R.C. Brower *et al.* (LSD Collaboration), *Phys. Rev.* **D 90** (2014) 014503 [arXiv:1403.2761 [hep-lat]].

[11] R. Brower, S. Chandrasekharan, J.W. Negele and U.-J. Wiese, *Phys. Lett.* **B 560** (2003) 64 [hep-lat/0302005].

[12] L. Del Debbio, L. Giusti and C. Pica, *Phys. Rev. Lett.* **94** (2005) 032003 [hep-th/0407052]. W. Bietenholz and S. Shcheredin, *Nucl. Phys.* **B 754** (2006) 17 [hep-lat/0605013]. S. Dürr, Z. Fodor, C. Hoelbling and T. Kurth, *JHEP* **0704** (2007) 055 [hep-lat/0612021].

[13] W. Bietenholz, R. Brower, S. Chandrasekharan and U.-J. Wiese, *Phys. Lett.* **B 407** (1997) 283 [hep-lat/9704015].

[14] W. Bietenholz, I. Hip, S. Shcheredin and J. Volkholz, *Eur. Phys. J.* **C 72** (2012) 1938 [arXiv:1109.2649 [hep-lat]].

[15] S. Aoki *et al.* (JLQCD and TWQCD Collaborations), *Phys. Lett.* **B 665** (2008) 294 [arXiv:0710.1130 [hep-lat]].

[16] H. Fukaya, S. Aoki, G. Cossu, S. Hashimoto, T. Kaneko and J. Noaki (JLQCD Collaboration), arXiv:1411.1473 [hep-lat].

[17] I. Bautista, W. Bietenholz, U. Gerber, C.P. Hofmann, H. Mejía-Díaz and L. Prado, arXiv:1402.2668 [hep-lat]. U. Gerber, I. Bautista, W. Bietenholz, H. Mejía-Díaz and C.P. Hofmann, arXiv:1410.0426 [hep-lat].

[18] N. Manton, *Phys. Lett.* **B 96** (1980) 328.

[19] W. Bietenholz, U. Gerber, M. Pepe and U.-J. Wiese, *JHEP* **1012** (2010) 020 [arXiv:1009.2146 [hep-lat]].

[20] A. Dromard and M. Wagner, *Phys. Rev.* **D 90** (2014) 074505 [arXiv:1404.0247 [hep-lat]].

[21] T. Boyer, W. Bietenholz and J. Wuilloud, *Int. J. Mod. Phys.* **C 18** (2007) 1497 [cond-mat/0701331].

[22] E. Seiler and I.O. Stamatescu, preprint MPI-PAE/PTh 10/87. E. Vicari, *Nucl. Phys.* **B 554** (1999) 301 [hep-lat/9901008]. E. Seiler, *Phys. Lett.* **B 525** (2002) 355 [hep-th/0111125].